HELDA
HELSINGIN YLIOPISTO
HELSINGFORS UNIVERSITET
UNIVERSITY OF HELSINKI

UNIVERSITY OF HELSINKI

https://helda.helsinki.fi

Influence of head positioning during cone-beam CT imaging on the accuracy of virtual 3D models

van Eijnatten, Maureen

2022-09-01

van Eijnatten , M , Wolff , J , Pauwels , R , Karhu , K , Hietanen , A , Sarkissian , H D & Koivisto , J H 2022 , ' Influence of head positioning during cone-beam CT imaging on the accuracy of virtual 3D models ' , Dentomaxillofacial Radiology , vol. 51 , no. 7 , 20220104 . https://doi.org/10.1259/dm

http://hdl.handle.net/10138/351254
https://doi.org/10.1259/dmfr.20220104

cc_by_nc
publishedVersion

Downloaded from Helda, University of Helsinki institutional repository.

This is an electronic reprint of the original article.

This reprint may differ from the original in pagination and typographic detail.

Please cite the original version.

Dentomaxillofacial Radiology (2022) 51, 20220104
© 2022 The Authors. Published by the British Institute of Radiology under the terms of the Creative Commons Attribution-NonCommercial 4.0 Unported License http://creativecommons.org/licenses/by-nc/4.0/, which permits unrestricted non-commercial reuse, provided the original author and source are credited.

birpublications.org/dmfr

RESEARCH ARTICLE

Influence of head positioning during cone-beam CT imaging on the accuracy of virtual 3D models

[1]Maureen van Eijnatten, [2]Jan Wolff, [3,4]Ruben Pauwels, [5]Kalle Karhu, [6]Ari Hietanen, [7]Henry der Sarkissian and [8]Juha H Koivisto

[1]Department of Oral and Maxillofacial Surgery/Oral Pathology, 3D Innovation Lab, Amsterdam UMC (location: VUmc), Amsterdam, The Netherlands; [2]Department of Dentistry and Oral Health Section of Oral and Maxillofacial Surgery and Oral Pathology, Aarhus University Vennelyst Boulevard , Aarhus C, Denmark; [3]Aarhus Institute of Advanced Studies Aarhus University Høegh-Guldbergs Gade 6B, Aarhus, Denmark; [4]Department of Radiology, Faculty of Dentistry, Chulalongkorn University, Bangkok, Thailand; [5]Varjo Oy Vuorikatu 20, FIN-00100, Helsinki, Finland; [6]Planmeca Oy Asentajankatu 6, FIN-00880, Helsinki, Finland; [7]Centrum Wiskunde & Informatica, Amsterdam, The Netherlands; [8]Department of Physics, University of Helsinki Gustaf Hällströmin katu 2, Helsinki, Finland

Objective: Cone beam computed tomography (CBCT) images are being increasingly used to acquire three-dimensional (3D) models of the skull for additive manufacturing purposes. However, the accuracy of such models remains a challenge, especially in the orbital area. The aim of this study is to assess the impact of four different CBCT imaging positions on the accuracy of the resulting 3D models in the orbital area.
Methods: An anthropomorphic head phantom was manufactured by submerging a dry human skull in silicon to mimic the soft tissue attenuation and scattering properties of the human head. The phantom was scanned on a ProMax 3D MAX CBCT scanner using 90 and 120 kV for four different field of view positions: standard; elevated; backwards tilted; and forward tilted. All CBCT images were subsequently converted into 3D models and geometrically compared with a "gold-standard" optical scan of the dry skull.
Results: Mean absolute deviations of the 3D models ranged between 0.15 ± 0.11 mm and 0.56 ± 0.28 mm. The elevated imaging position in combination with 120 kV tube voltage resulted in an improved representation of the orbital walls in the resulting 3D model without compromising the accuracy.
Conclusions: Head positioning during CBCT imaging can influence the accuracy of the resulting 3D model. The accuracy of such models may be improved by positioning the region of interest (*e.g.* the orbital area) in the focal plane (Figure 2a) of the CBCT X-ray beam.
Dentomaxillofacial Radiology (2022) **51**, 20220104. doi: 10.1259/dmfr.20220104

Cite this article as: van Eijnatten M, Wolff J, Pauwels R, Karhu K, Hietanen A, der Sarkissian H, et al. Influence of head positioning during cone-beam CT imaging on the accuracy of virtual 3D models. *Dentomaxillofac Radiol* (2022) 10.1259/dmfr.20220104.

Keywords: Cone-Beam Computed Tomography; Orbit; Dimensional Measurement Accuracy; Printing; Three-Dimensional

Introduction

Over the past decade, advances in image analysis and graphics processing power have extended the role of medical imaging far beyond traditional, diagnostic visualization. Three-dimensional (3D) medical images are being increasingly used to additively manufacture patient-specific constructs, such as anatomical models, surgical cutting guides and implants.[1,2] Such patient-specific constructs have proven to be particularly valuable in the field of oral and maxillofacial surgery and

Correspondence to: Juha H Koivisto, E-mail: juha.koivisto@planmeca.com
Received 17 March 2022; revised 06 June 2022; accepted 27 June 2022; published online 06 July 2022

are being increasingly used to reconstruct the orbit after trauma.[3–5]

The current medical additive manufacturing (AM) process comprises three basic steps. The first step is image acquisition, which is commonly performed using a CT scanner. The second step is image processing, during which the tissue of interest is segmented in the CT images and converted into a 3D model by means of meshing. The resulting 3D model is commonly saved as a standard tessellation language (STL) file that can subsequently be used to design patient-specific constructs, such as orbital floor implants, using dedicated computer-aided design (CAD) software. The third and final step in the medical AM process is the fabrication of the construct using a 3D printer.[6]

While the aforementioned medical constructs can be fabricated with great accuracy (<0.1 mm) using current 3D printing technologies, their design is limited by the accuracy of the medical images.[7,8]

To date, there is a general agreement that multislice CT (MSCT) scanners offer the best images for medical AM.[9] However, cone beam CT (CBCT) scanners are being increasingly used for dentomaxillofacial imaging due to their high sharpness, low costs and low radiation dose.[10] Consequently, an increasing number of patient-specific 3D constructs are being designed using CBCT images. This development has sparked the need to optimize CBCT for the generation of 3D models suitable for medical AM.

One key limitation of using CBCT images for medical AM is the fact that thin and complex bony structures, such as the orbital walls, are often poorly represented in CBCT-derived 3D models.[11] This is mostly due to the beam geometry and image acquisition strategies used in CBCT imaging. Furthermore, the scaffold-like structures of the eye socket are surrounded by thick bony structures such as zygoma that predominantly attenuate the low-energy part of the X-ray spectrum by causing both beam hardening and photon "starvation". The remaining high-energy photons are less likely to become absorbed by the thin bone structures resulting in a contrast loss and difficulty to separate transitions between bone and soft tissues thus making STL models challenging. However, the attenuation caused by the thick bony structures can be partially avoided by choosing an exposure orientation that offers minimal bone mass in the radiation path. CBCT scanners irradiate the entire field of view (FOV) during a single (full or partial) gantry rotation using a wide X-ray beam in combination with a single, flat-panel detector. Consequently, the irradiation reduces contrast of the image by causing a large non-uniform background exposure. The magnitude of this so-called scatter-to-primary ratio is defined as scatter radiation intensity divided by primary radiation intensity at the level of the detector. The resulting large beam angles induce high scatter-to-primary ratios, which manifests in the reconstructed images as reduced contrast between different tissue types.[12] Although such low contrast-to-noise ratios (CNRs) typically do not hinder the diagnostic use of CBCT images for tissues with high anatomical contrast (*e.g.* bone, teeth, air spaces), they make CBCT image segmentation notably more cumbersome in the field of medical AM.[13,14]

The extent to which the CNR is impacted by imaging a specific anatomical structure of interest (*e.g.* the orbits) depends on its position in the FOV during CBCT imaging.

Various studies have shown that head positioning in the CBCT scanner can influence the accuracy of linear measurements, CNR, and other image quality figures of merit.[15,16] Furthermore, a recent study by Lindfors et al reported that tilting the head backwards resulted in significantly higher mean CNR in two different CBCT scanners.[17] These findings suggest that CBCT images could be optimized for medical AM by adapting the position of the anatomical structure of interest in the FOV of the CBCT scanner. However, to the best of the authors' knowledge, the combination of head tilting and positioning has not been previously investigated. Therefore, the aim of the present study is to assess the impact of four different CBCT imaging positions on the accuracy of the resulting 3D models in the orbital area using an anthropomorphic head phantom.

Methods and materials

Manufacturing of an anthropomorphic head phantom

This study was performed according to the Ethical Principles for Medical Research Involving Human Subjects as defined by the World Medical Association.[18] One female human cadaver head was anonymously provided by the Department of Anatomy, Amsterdam UMC (location VUmc), Amsterdam, The Netherlands. The head was boiled for 24 h, after which all remaining soft tissues were manually removed using standard dissection equipment (*i.e.* scrapers and scalpels). The resulting dry skull was subsequently scanned using a GOM ATOS™ III optical 3D scanner (GOM GmbH, Braunschweig, Germany) with an accuracy of 0.05 mm to acquire an accurate "gold-standard" 3D model of the skull.[19] The scanned dry skull was placed in a head-shaped mould that was milled using a CNC 5-axis milling machine (Figure 1). This mould was subsequently filled with silicone (Dragon Skin® 30, Smooth-On, Macungie, PA, $\rho = 1.08\,g/cm^3$) to mimic the attenuation and scattering conditions of soft tissues in the human head. The major advantages of Dragon Skin silicone are its elasticity that allows easy moulding, stability at room temperature, long shelf life and fast curing time (<16 h).

Image acquisition

The phantom head was scanned in four different imaging positions using a Planmeca ProMax 3D Max CBCT scanner (Planmeca, Helsinki, Finland) with a

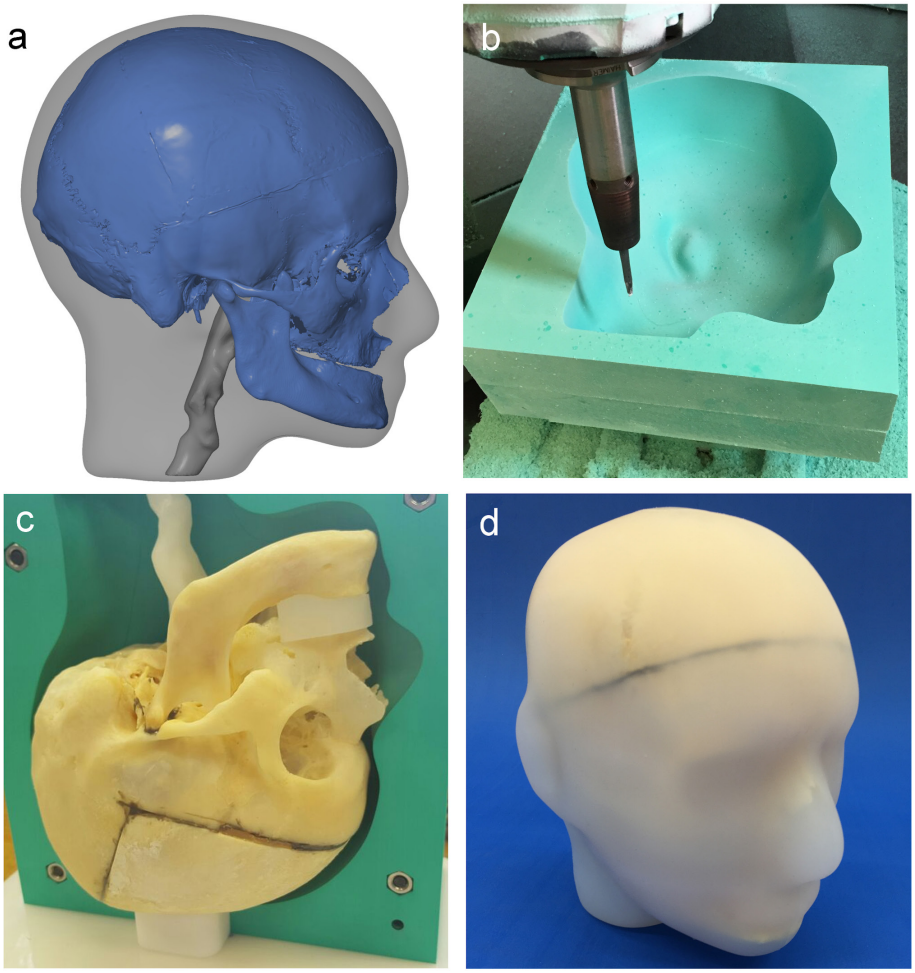

Figure 1 Manufacturing of the anthropomorphic head phantom. (a) Computer-aided design of the dry skull embedded in a head-shaped cast; (b) milling of the mold; (c) the dry skull positioned in the mold; and (d) the resulting head phantom cast in silicon.

230 × 160 mm FOV. The first position was the standard imaging protocol on the ProMax 3D Max CBCT scanner, in which the FOV extended from the tip of the chin to the forehead (Figure 2a). The three other imaging positions were achieved by elevating the FOV so that the focal plane intersected with the orbital floors (Figure 2b), by additionally tilting the elevated phantom head backwards (−45°) (Figure 2c), and by tilting the phantom head forward (+45°) (Figure 2d). In the current set-up, the focal plane is defined as a horizontal plane at the position where the X-ray beam emerging from the focal spot reaches the detector perpendicularly. All CBCT scans were performed using two different scanning protocols with similar effective doses: 90 kV, 14 mA and 120 kV, 5.6 mA. The exposure time for both protocols was 7.8 s. The ProMax 3D Max CBCT scanner uses asymmetric imaging geometry that minimizes the radiation dose to thyroid gland for large FOVs. However, the physical phenomenon resulting from the head tilting remains regardless of the CBCT scanner used.

Image processing

All acquired CBCT scans were reconstructed as Digital Imaging and Communications in Medicine (DICOM) data sets with 0.4 mmx0.4 mm x 0.4 mm voxels. The acquired DICOM data sets were subsequently imported into Mimics 3D medical image processing software (v. 20, Materialise, Leuven, Belgium), and all bony structures in the CBCT images were segmented using global thresholding. (Semi-)automatic image segmentation techniques such as automatic threshold selection or region growing, however, lead to suboptimal segmentation results for these types of relatively noisy CBCT images. Therefore, we jointly optimized the threshold value for all CBCT scans that were acquired using a specific tube voltage (90 and 120 kV). To eliminate bias and enable a fair comparison between the CBCT scans acquired using different head positions, we opted for one threshold value that was suitable for all four head positions. This threshold value was determined by drawing intensity value profile lines through the zygoma and the medial orbital walls at axial slices representing

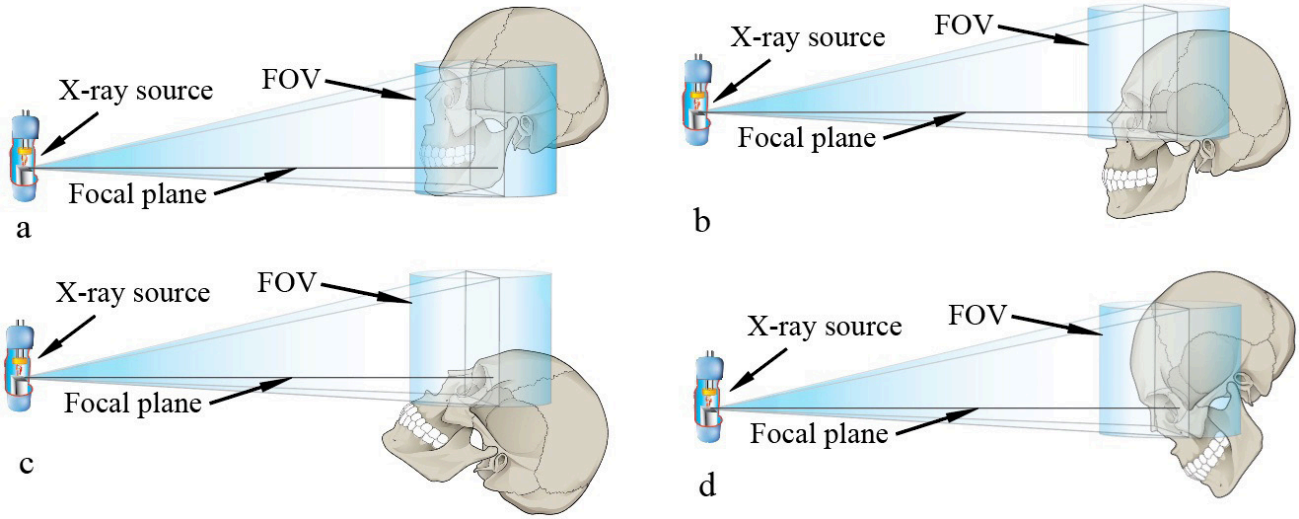

Figure 2 (a) Standard FOV; (b) elevated FOV; (c) elevated FOV and backwards (−45°) tilted; and (d) elevated FOV and forward (+45°) tilted. FOV, field of view.

the same craniocaudal level for each CBCT scan. Based on these profile lines, an observer selected the optimal threshold value such that the resulting segmentation included as many bone voxels of the orbital walls as possible without including connected soft-tissue voxels and noise. The optimized thresholds were subsequently averaged over the four scans, resulting in a threshold value of 621 for the 90 kV scans and a threshold value of 566 for the 120 kV scans.

After segmentation of the bony structures, all segmented CBCT scans were converted into 3D models and exported as STL files. These 3D models were imported into GOM Inspect metrology software (GOM GmbH, Braunschweig, Germany) and the noise-residuals and unconnected triangles were removed. All acquired 3D models were geometrically aligned with the "gold-standard" 3D model of the dry skull that was acquired with the optical scanner. The alignments were performed using a manual 3-point alignment, followed by a local best-fit using a maximum search distance of 5.0 mm in GOM Inspect software. Finally, the geometric deviations between all CBCT-derived 3D models and the gold-standard 3D model were calculated using the surface comparison functionality in GOM Inspect. This surface comparison function calculates the shortest perpendicular distance between a polygon point of the CBCT-derived 3D models and the gold-standard 3D model. This was performed for each polygon point of the CBCT-derived 3D model. Note that the deviations can be expressed at subvoxel-level accuracy due to the use of triangulated surface models, which are not bound by the voxel size. The resulting surface deviations were superimposed on the CBCT-derived 3D models using color maps (Figures 3 and 4).

Orbit bone fill factor

In order to quantify the representation of the orbital walls in the 3D models, orbital bone fill factors were calculated as follows. The orbits were cut out of all 3D models and halved using a mid-orbital axial plane in GOM Inspect software (Figure 5). The orbital floor was subsequently projected onto the mid-orbital axial plane. Note that this method was also applied to the laser-scanned 3D model in order to obtain a 'gold-standard projection'. The orbital bone fill factor was calculated as the surface area (in mm^2 of the CBCT-derived projection (Figure 5) divided by the surface area (in mm^2 of the gold standard projection (Figure 5a), expressed as a percentage. To assess the reproducibility of the method, 10 CBCT scans were consecutively acquired in the standard imaging position (Figure 2a) and the elevated imaging position using a tube voltage of 120 kV.

Results

The geometric deviations of the 3D models acquired in four different phantom positions (Figure 2) are presented in Figures 3 and 4. The mean absolute deviations of the 3D models acquired using a tube voltage of 90 kV ranged between 0.15 ± 0.11 mm and 0.42 ± 0.31 mm, whilst the mean absolute deviations of the 120 kV 3D models ranged between 0.17 ± 0.13 mm and 0.56 ± 0.28 mm (Table 1). The orbital bones demonstrated larger geometric deviations (0.41 ± 0.25 mm) than the cranial bones (0.20 ± 0.15 mm). The mean absolute deviations resulting from the four different imaging positions were 0.33 ± 0.21 mm (standard), 0.30 ± 0.19 mm (elevated), 0.32 ± 0.20 mm (backward tilted) and 0.26 ± 0.19 mm (forward tilted).

The representation of the orbits in all 3D models was quantified using the "orbital bone fill factor" (Figure 5).

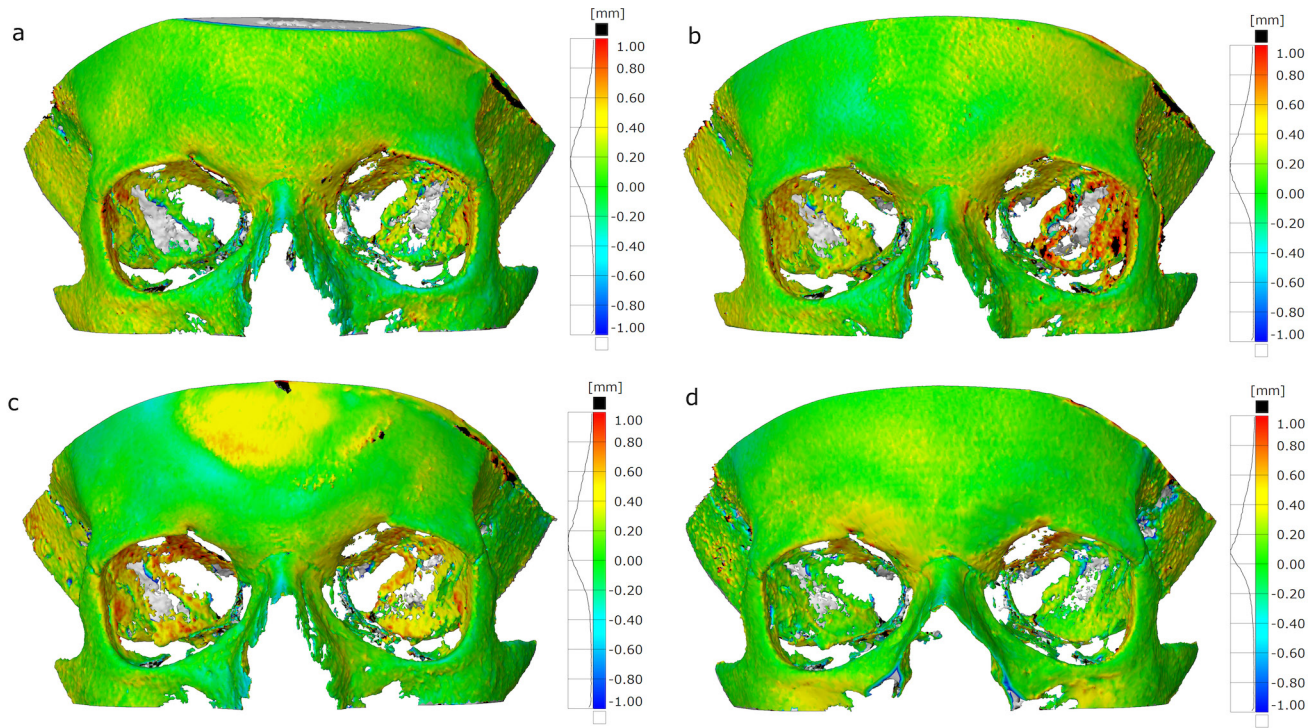

Figure 3 3D models obtained using a CBCT tube voltage of 90 kV in four positions: (a) standard FOV; (b) elevated FOV; (c) elevated FOV and backwards (−45°) tilted; and (d) elevated FOV and forward (+45°) tilted. CBCT, cone beam CT; FOV, field of view.

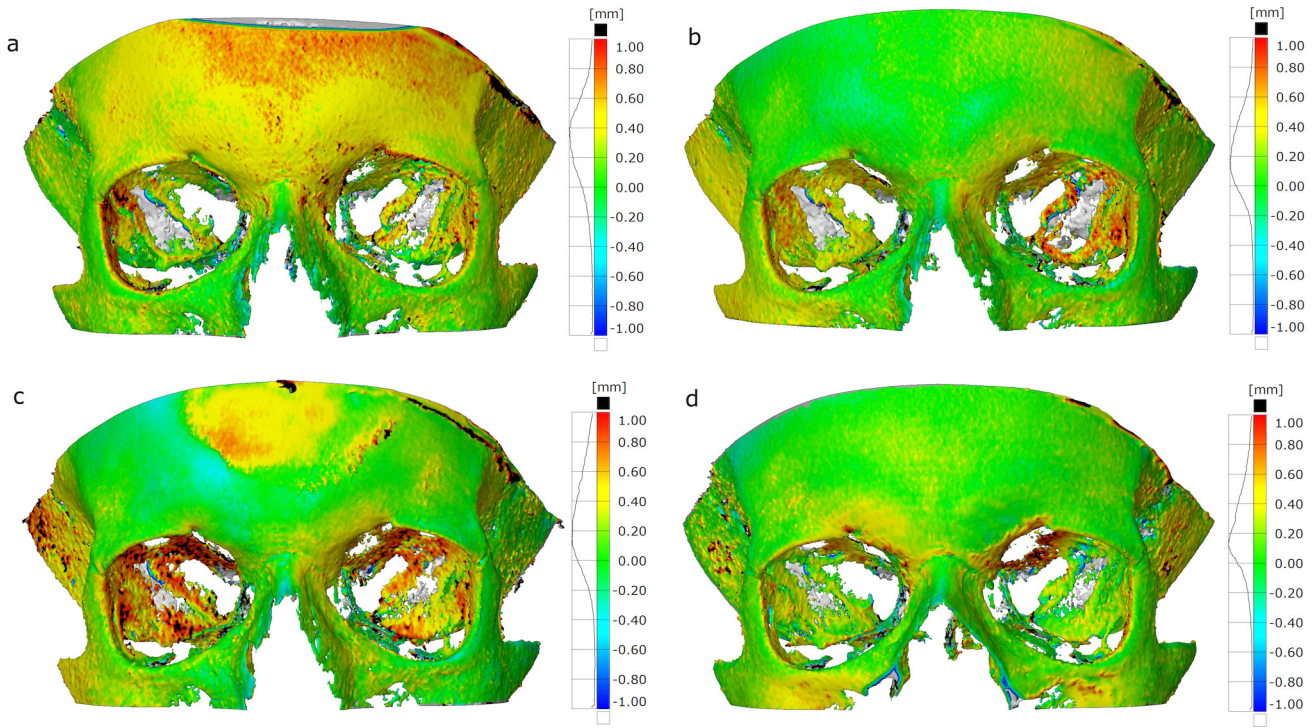

Figure 4 3D models acquired using a CBCT tube voltage of 120 kV in four positions: (a) standard FOV; (b) elevated FOV; (c) elevated FOV and backwards (−45°) tilted; and d) elevated FOV and forward (+45°) tilted. 3D, three-dimensional; CBCT, cone beam CT; FOV, field of view.

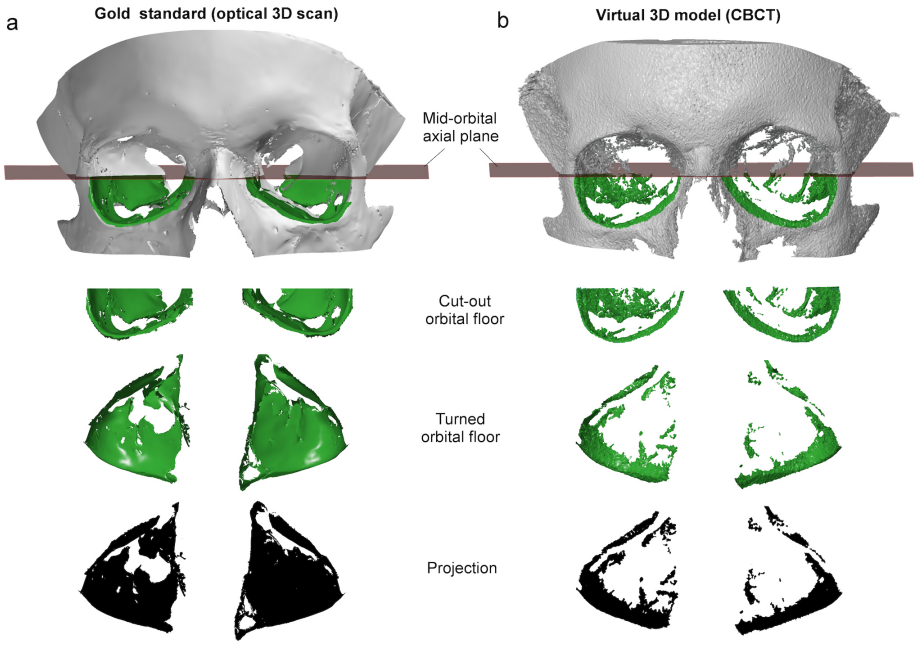

Figure 5 Calculation of the orbital bone fill factor. (a) Gold-standard 3D model of the orbital floor; and (b) an example of a CBCT-derived 3D model of the orbital floor with the corresponding projections onto the mid-orbital axial plane. The orbital bone fill factor is defined as the ratio between the CBCT-derived projection (b) and the gold-standard projection (a). 3D, three-dimensional; CBCT, cone beam CT.

When compared to the standard imaging position (Figure 2a), lowering the phantom head in the CBCT X-ray beam (Figure 2b) increased the orbital bone fill factor in all 3D models from 67.0 to 75.3% (90 kV) and from 69.1 to 76.3% (120 kV) (Figure 6). In the 3D models acquired using 120 kV, tilting the head backwards or forward improved the orbital bone fill factor to 84.0 and 80.2%, respectively. On the other hand, when using a 90 kV tube current, these imaging positions resulted in fill factors of 70.8% (backward tilted, Figure 2c) and 75.0% (forward tilted, Figure 2d), which was lower than the 75.3% achieved using the elevated imaging position.

Table 1 Mean absolute deviations and SD of the orbital and cranial bones in the CBCT-derived 3D models

			90 kV	*120 kV*
	Phantom position	***Anatomical structure***	*Mean absolute deviation (mm) ± SD (mm)*	*Mean absolute deviation (mm) ± SD (mm)*
a)	Standard FOV	Orbit	0.38 ± 0.25	0.39 ± 0.20
		Cranium	0.18 ± 0.19	0.38 ± 0.19
b)	Elevated FOV	Orbit	0.42 ± 0.31	0.40 ± 0.19
		Cranium	0.19 ± 0.14	0.17 ± 0.13
c)	Elevated FOV and backwards (+45°) tilted	Orbit	0.39 ± 0.24	0.56 ± 0.28
		Cranium	0.15 ± 0.13	0.18 ± 0.15
d)	Elevated FOV and forward (−45°) tilted	Orbit	0.32 ± 0.24	0.40 ± 0.26
		Cranium	0.15 ± 0.11	0.17 ± 0.15

CBCT, cone beam CT; FOV, field of view; SD, standard deviation.

Figure 7 demonstrates the reproducibility of the orbital bone fill factor experiment. The standard deviation of the orbital bone fill factor was 1.9% for the standard imaging position and 1.2% for the elevated imaging position.

Discussion

To date, CBCT images are not commonly used to additively manufacture anatomical models and implants due to inaccuracies and data loss in CBCT-derived 3D models. This data loss particularly occurs in anatomical

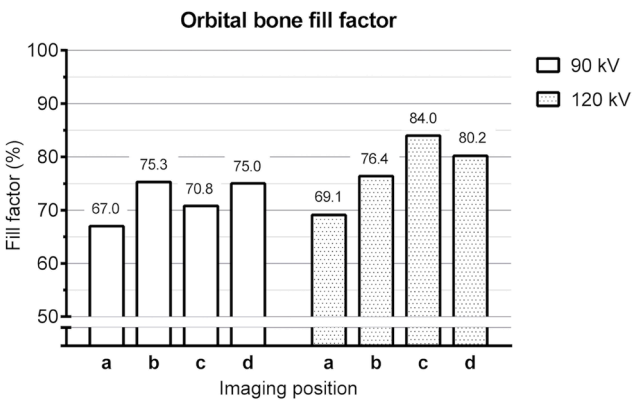

Figure 6 Orbital bone fill factor of the eight 3D models acquired using a tube voltage of 90 kV and 120 kV in four different imaging positions: (a) standard FOV; (b) elevated FOV; (c) elevated FOV and backwards (−45°) tilted; and (d) elevated FOV and forward (+45°) tilted. 3D, three-dimensional; FOV, field of view.

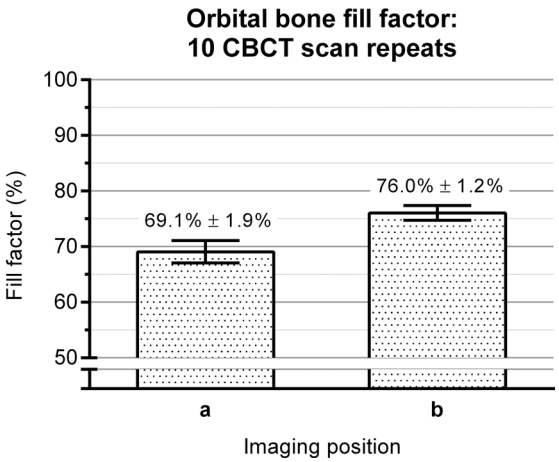

Figure 7 Orbital bone fill factor of ten 3D models acquired using a tube voltage of 120 kV in two different imaging positions: (a) standard FOV; and (b) elevated FOV. 3D, three-dimensional; CBCT, cone beam CT; FOV, field of view.

areas that comprise thin and complex bony structures, such as the orbits. Therefore, the aim of the present study was to investigate the effect of head positioning (elevating the FOV and tilting the head backwards and forward) during CBCT imaging on the accuracy of 3D models in the orbital area.

The orbital bone fill factors of the 3D models acquired using four different CBCT imaging positions are presented in Figure 6. All lowered phantom positions (Figure 2b) resulted in higher orbital bone fill factors, *i.e.* a more complete representation of the orbital bones. This is possibly due to the reduction of high cone-angle artifacts. These artifacts result from violating Tuy's sufficiency condition, which requires that each plane intersecting a reconstructed region of interest must intersect the focal trajectory, *i.e.* the path defining the radiation source position during imaging.[20] In practice, this means that the best CBCT image quality is obtained in the focal plane (Figure 2a). Outside of the focal plane, Tuy's sufficiency condition is not satisfied, which leads to image degradation as the axial distance to the focal plane increases.[13,21,22] An additional reason for image quality degradation is the increased beam path length at higher beam angles—the X-rays have more tissue to traverse, resulting in higher attenuation and thus potentially higher scatter-to-primary ratios. This results in reconstructions that have globally more noise and reduced contrast, as well as an increased degree of streak-like artifacts. Although the resulting image quality degradation can be reduced to some extent using artifact correction algorithms, complete correction remains a challenge.[23–25] It should also be noted that the artifacts are especially pronounced when the reconstruction algorithm of choice involves filtered backprojection (FBP), which still is the most widespread reconstruction method in CBCT due to its simplicity and fast reconstruction times.[26,27]

Another finding in this study was that the bone fill factors acquired in the standard (Figure 2a) and lowered phantom positions (Figure 2b) did not depend on the tube voltage, whereas in the backwards-tilted imaging position (Figure 2c) a change in the tube voltage from 90 to 120 kV resulted in a relative improvement in bone fill factor of 13.2%. A potential contributing factor to this increase could be the fact that photons generated using 120 kV are less attenuated by the thick maxillary bones surrounding the orbits, resulting in higher signal levels on the detector.

Higher signals decrease the effect of both the quantum noise and electrical noise of the detector, and thereby enhance the contrast in the orbital floor area. On the other hand, at higher tube voltages the probability of absorption within the flat panel decreases, which can have a negative impact on the CNR. In the forward-tilted imaging position (Figure 2d), the bone fill factor acquired using a 120 kV tube voltage was only 5.2% higher than the bone fill factor acquired using 90 kV. This difference between the backward tilted position (Figure 2d) and the forward tilted position (Figure 2c) can be attributed to the amount of scatter: in the backwards tilted position since the skull is only partially covered by the FOV (Figure 2), which reduces scatter, and thereby improves image quality.

This study demonstrates that matching the orbital floor with the focal plane (Figure 2a) of the CBCT scanner improves the segmentation accuracy of the resulting images. Further improvements in the orbital bone fill factor could be achieved by developing novel image segmentation methods that can better handle the higher scatter-to-primary ratios and geometrical high cone-angle artefacts inherent to CBCT technology. In this context, recent studies have reported very promising results using deep learning.[28–30]

Clinical implications

Good representation of the orbits in 3D models is pivotal for the design and manufacturing of accurate patient-specific orbital implants.[3] A poor fit of an implant to the patient's anatomy can lead to increased movements of the implant, which may impede tissue repair and subsequently lead to complications after surgery.[31] However, the orbits remain difficult to depict and segment on CBCT images due to the very thin (<1 mm) bony structures found in this area. In the present study, the highest orbital bone fill factor of all CBCT-derived 3D models was acquired using the elevated FOV (Figure 2b) and backwards tilted imaging position (Figure 2c) in combination with a tube voltage of 120 kV (Figure 6). However, this imaging position also resulted in a slight increase in mean absolute deviation in the orbital area (Table 1). On the other hand, the elevated imaging position together with 120 kV tube voltage resulted in a relative increase in orbital bone fill factor of 10.6% without compromising the accuracy of the 3D model in the orbital and cranial area.

Furthermore, this elevated imaging position is relatively easy to implement in clinical settings using conventional CBCT scanners. The CBCT scanner of the current study, however, uses asymmetric imaging geometry and the upper part of the FOV is prone for larger geometrical distortions when compared to the lower part of the FOV. The physical phenomenon resulting from the head tilting, however, is independent of the CBCT scanner used, although the optimal tilting angle may depend on the exact beam geometry.

Taking the aforementioned findings into account, we recommend to position the anatomical structure of interest in the focal plane of the CBCT X-ray beam when acquiring images for medical AM purposes. Finally, note that the geometric deviations found in the orbital area (0.41 ± 0.25 mm) were generally larger than the geometric deviations of the cranial bones (0.20 ± 0.15 mm). We suggest that engineers and clinical professionals should take these inaccuracies into account when designing patient-specific orbital floor implants.

Limitations of this study

One limitation of the present study was that the anthropomorphic phantom head was not fully identical to a real patient since all soft tissues were mimicked by a material with a uniform density, namely silicon. Also, the edentulous skull could have an impact on beam hardening. However, in the present study the radiation path of different scanning directions did not penetrate through the dentoalveolar area; thus, the absence of teeth did not have an impact on the results. Furthermore, in clinical settings one can expect motion artefacts due to breathing and small patient movements. Therefore, the reported accuracies found in this study are not directly generalizable to clinical conditions.

Conclusions

This study demonstrates that phantom head positioning during CBCT imaging can influence the accuracy and completeness of 3D models of the skull. Elevating the FOV when using a 120 kV tube voltage improves the representation of the orbital bones in the resulting 3D model for medical AM purposes without compromising the accuracy.

Acknowledgements

Ruben Pauwels is supported by the European Union Horizon 2020 Research and Innovation Programme under the Marie Skłodowska-Curie grant agreement number 754513 and by Aarhus University Research Foundation (AIAS-COFUND).

Conflict of interest

The authors have no relevant conflicts of interest to disclose.

REFERENCES

1. Ventola CL. Medical applications for 3D printing: current and projected uses. *P T* 2014; **39**: 704–11.
2. Rengier F, Mehndiratta A, von Tengg-Kobligk H, Zechmann CM, Unterhinninghofen R, Kauczor H-U, et al. 3D printing based on imaging data: review of medical applications. *Int J Comput Assist Radiol Surg* 2010; **5**: 335–41. https://doi.org/10.1007/s11548-010-0476-x
3. Stoor P, Suomalainen A, Lindqvist C, Mesimäki K, Danielsson D, Westermark A, et al. Rapid prototyped patient specific implants for reconstruction of orbital wall defects. *J Craniomaxillofac Surg* 2014; **42**: 1644–49. https://doi.org/10.1016/j.jcms.2014.05.006
4. Kozakiewicz M. Computer-aided orbital wall defects treatment by individual design ultrahigh molecular weight polyethylene implants. *J Craniomaxillofac Surg* 2014; **42**: 283–89. https://doi.org/10.1016/j.jcms.2013.05.015
5. Gander T, Essig H, Metzler P, Lindhorst D, Dubois L, Rücker M, et al. Patient specific implants (PSI) in reconstruction of orbital floor and wall fractures. *J Craniomaxillofac Surg* 2015; **43**: 126–30. https://doi.org/10.1016/j.jcms.2014.10.024
6. Mitsouras D, Liacouras P, Imanzadeh A, Giannopoulos AA, Cai T, Kumamaru KK, et al. Medical 3D printing for the radiologist. *Radiographics* 2015; **35**: 1965–88. https://doi.org/10.1148/rg.2015140320
7. Pinto JM, Arrieta C, Andia ME, Uribe S, Ramos-Grez J, Vargas A, et al. Sensitivity analysis of geometric errors in additive manufacturing medical models. *Med Eng Phys* 2015; **37**: 328–34. https://doi.org/10.1016/j.medengphy.2015.01.009
8. van Eijnatten M, Berger FH, de Graaf P, Koivisto J, Forouzanfar T, Wolff J. Influence of CT parameters on STL model accuracy. *RPJ* 2017; **23**: 678–85. https://doi.org/10.1108/RPJ-07-2015-0092
9. Liang X, Lambrichts I, Sun Y, Denis K, Hassan B, Li L, et al. A comparative evaluation of cone beam computed tomography (CBCT) and multi-slice CT (MSCT). part II: on 3D model accuracy. *Eur J Radiol* 2010; **75**: 270–74. https://doi.org/10.1016/j.ejrad.2009.04.016
10. Pauwels R, Beinsberger J, Collaert B, Theodorakou C, Rogers J, Walker A, et al. Effective dose range for dental cone beam computed tomography scanners. *Eur J Radiol* 2012; **81**: 267–71. https://doi.org/10.1016/j.ejrad.2010.11.028
11. Bakhtiar SM, Butt HA, Zeb S, Quddusi DM, Gul S, Dilshad E. (n.d.). Eds. omics technologies and bio-engineering. *Academic Press*; **2018**: 167–89. https://doi.org/10.1016/B978-0-12-804659-3.00010-5
12. Pauwels R, Pittayapat P, Sinpitaksakul P, Panmekiate S. Scatter-to-primary ratio in dentomaxillofacial cone-beam CT: effect of field of view and beam energy. *Dentomaxillofac Radiol* 2021; **50**(8): 20200597. https://doi.org/10.1259/dmfr.20200597
13. Mori S, Endo M, Obata T, Tsunoo T, Susumu K, Tanada S. Properties of the prototype 256-row (cone beam) CT scanner. *Eur Radiol* 2006; **16**: 2100–2108. https://doi.org/10.1007/s00330-006-0213-6
14. van Eijnatten M, Koivisto J, Karhu K, Forouzanfar T, Wolff J. The impact of manual threshold selection in medical additive manufacturing. *Int J Comput Assist Radiol Surg* 2017; **12**: 607–15. https://doi.org/10.1007/s11548-016-1490-4

15. Adibi S, Shahidi S, Nikanjam S, Paknahad M, Ranjbar M. Influence of head position on the CBCT accuracy in assessment of the proximity of the root apices to the inferior alveolar canal. *J Dent Shiraz, Iran* 2017; **18**: 181–86.
16. Koivisto J, van Eijnatten M, Järnstedt J, Holli-Helenius K, Dastidar P, Wolff J. Impact of prone, supine and oblique patient positioning on CBCT image quality, contrast-to-noise ratio and figure of merit value in the maxillofacial region. *Dentomaxillofac Radiol* 2017; **46**(6): 20160418. https://doi.org/10.1259/dmfr.20160418
17. Lindfors N, Lund H, Johansson H, Ekestubbe A. Influence of patient position and other inherent factors on image quality in two different cone beam computed tomography (CBCT) devices. *Eur J Radiol Open* 2017; **4**: 132–37. https://doi.org/10.1016/j.ejro.2017.10.001
18. World Medical Association. World medical association declaration of helsinki: ethical principles for medical research involving human subjects. *JAMA* 2013; **310**: 2191–94. https://doi.org/10.1001/jama.2013.281053
19. Kersten TP, Lindstaedt M, Starosta D. COMPARATIVE geometrical accuracy investigations of hand-held 3D scanning systems – an update. *Int Arch Photogramm Remote Sens Spatial Inf Sci* 2018; **XLII–2**: 487–94. https://doi.org/10.5194/isprs-archives-XLII-2-487-2018
20. Tuy HK. An inversion formula for cone-beam reconstruction. *SIAM J Appl Math* 1983; **43**: 546–52. https://doi.org/10.1137/0143035
21. Schulze R, Heil U, Gross D, Bruellmann DD, Dranischnikow E, Schwanecke U, et al. Artefacts in CBCT: a review. *Dentomaxillofac Radiol* 2011; **40**: 265–73. https://doi.org/10.1259/dmfr/30642039
22. Kalender WA, Kyriakou Y. Flat-detector computed tomography (FD-CT). *Eur Radiol* 2007; **17**: 2767–79. https://doi.org/10.1007/s00330-007-0651-9
23. Zeng K, Chen Z, Zhang L, Wang G. An error-reduction-based algorithm for cone-beam computed tomography. *Med Phys* 2004; **31**: 3206–12. https://doi.org/10.1118/1.1809792
24. Maaß C, Dennerlein F, Noo F, Kachelrieß M. *In: Nuclear Science Symposium Conference Record (NSS/MIC), 2010 IEEE*; **2010**: 2188–93.
25. Hsieh J. A practical cone beam artifact correction algorithm. 2000 IEEE Nuclear Science Symposium. Conference Record; Lyon, France. Vol. 2000; 2000. pp. 15–71. https://doi.org/10.1109/NSSMIC.2000.950053
26. Feldkamp LA, Davis LC, Kress JW. Practical cone-beam algorithm. *J Opt Soc Am A* 1984; **1**: 612. https://doi.org/10.1364/JOSAA.1.000612
27. Pauwels R, Araki K, Siewerdsen JH, Thongvigitmanee SS. Technical aspects of dental CBCT: state of the art. *Dentomaxillofac Radiol* 2015; **44**(1): 20140224. https://doi.org/10.1259/dmfr.20140224
28. DeVries NA, Gassman EE, Kallemeyn NA, Shivanna KH, Magnotta VA, Grosland NM. Validation of phalanx bone three-dimensional surface segmentation from computed tomography images using laser scanning. *Skeletal Radiol* 2008; **37**: 35–42. https://doi.org/10.1007/s00256-007-0386-3
29. Moeskops P, Wolterink JM, vander, Velden BHM, Gilhuis KG, Leiner T, et al. Deep Learning for Multi-task Medical Image Segmentation in Multiple Modalities. In: Paper presented at the In: Paper presented at the In: Paper presented at the In International on Medical Image Computing and Computer-Assisted Intervention -- MICCAI 2016: 19th International Conference, , Proceedings, , Athens, Greece. https://doi.org/10.1007/978-3-319-46723-8_55
30. Litjens G, Kooi T, Bejnordi BE, Setio AAA, Ciompi F, Ghafoorian M, et al. A survey on deep learning in medical image analysis. *Med Image Anal* 2017; **42**: 60–88. https://doi.org/10.1016/j.media.2017.07.005
31. Lienau J, Schell H, Duda GN, Seebeck P, Muchow S, Bail HJ. Initial vascularization and tissue differentiation are influenced by fixation stability. *J Orthop Res* 2005; **23**: 639–45. https://doi.org/10.1016/j.orthres.2004.09.006